

NAQFC Developmental Forecast Guidance for Fine Particulate Matter (PM_{2.5})

PIUS LEE,^{a,b} JEFFERY MCQUEEN,^c IVANKA STAJNER,^d JIANPING HUANG,^{c,e} LI PAN,^{a,f} DANIEL TONG,^{a,b,f} HYUNCHEOL KIM,^{a,f} YOUHUA TANG,^{a,f} SHOBHA KONDRAGUNTA,^g MARK RUMINSKI,^h SARAH LU,ⁱ ERIC ROGERS,^c RICK SAYLOR,^a PERRY SHAFRAN,^{c,e} HO-CHUN HUANG,^{c,e} JERRY GORLINE,^j SIKCHYA UPADHAYAY,^{d,k} AND RICHARD ARTZ^a

^a NOAA/Air Resources Laboratory, NOAA Center for Weather and Climate Prediction, College Park, Maryland

^b Center for Spatial Information Science and Systems, George Mason University, Fairfax, Virginia

^c NOAA/NCEP/Environmental Modeling Center, NOAA Center for Weather and Climate Prediction, College Park, Maryland

^d NOAA/National Weather Service/Office of Science and Technology Integration, Silver Spring, Maryland

^e I.M. System Group, Rockville, Maryland

^f Cooperative Institute for Climate and Satellite, University of Maryland, College Park, College Park, Maryland

^g NOAA/NESDIS/Center for Satellite Applications and Research, College Park, Maryland

^h NOAA/NESDIS/Satellite Analysis Branch, NOAA Center for Weather and Climate Prediction, College Park, Maryland

ⁱ Atmospheric Sciences Research Center, University at Albany, State University of New York, Albany, New York

^j Meteorological Development Laboratory, Silver Spring, Maryland

^k Syneren Technologies Corporation, Arlington, Virginia

(Manuscript received 15 November 2015, in final form 4 July 2016)

ABSTRACT

The National Air Quality Forecasting Capability (NAQFC) upgraded its modeling system that provides developmental numerical predictions of particulate matter smaller than 2.5 μm in diameter (PM_{2.5}) in January 2015. The issuance of PM_{2.5} forecast guidance has become more punctual and reliable because developmental PM_{2.5} predictions are provided from the same system that produces operational ozone predictions on the National Centers for Environmental Prediction (NCEP) supercomputers.


There were three major upgrades in January 2015: 1) incorporation of real-time intermittent sources for particles emitted from wildfires and windblown dust originating within the NAQFC domain, 2) suppression of fugitive dust emissions from snow- and/or ice-covered terrain, and 3) a shorter life cycle for organic nitrate in the gaseous-phase chemical mechanism. In May 2015 a further upgrade for emission sources was included using the U.S. Environmental Protection Agency's (EPA) 2011 National Emission Inventory (NEI). Emissions for ocean-going ships and on-road mobile sources will continue to rely on NEI 2005.

Incremental tests and evaluations of these upgrades were performed over multiple seasons. They were verified against the EPA's AIRNow surface monitoring network for air pollutants. Impacts of the three upgrades on the prediction of surface PM_{2.5} concentrations show large regional variability: the inclusion of windblown dust emissions in May 2014 improved PM_{2.5} predictions over the western states and the suppression of fugitive dust in January 2015 reduced PM_{2.5} bias by 52%, from 6.5 to 3.1 $\mu\text{g m}^{-3}$ against a monthly average of 9.4 $\mu\text{g m}^{-3}$ for the north-central United States.

1. Introduction

Epidemiological studies indicate that ozone (O₃) and particulate matter smaller than 2.5 μm in diameter (PM_{2.5}) are among a handful of criteria air pollutants

that are primarily responsible for adverse impacts on human health (EPA 2005). Inhalation of these pollutants is recognized as a major cause of acute and chronic respiratory and cardiovascular diseases and air pollution-associated premature mortalities (e.g., Fann et al. 2012). The National Air Quality Forecasting Capability (NAQFC) is designed to safeguard the public by providing forecast guidance for surface concentrations of these pollutants at fine enough spatial and temporal resolutions and with sufficient lead times to be useful for official interpretative air quality forecasts issued by state and local air quality forecasters. NAQFC operational O₃ forecast

 Denotes Open Access content.

Corresponding author address: Pius Lee, NOAA/ARL/Air Quality and Atmospheric Chemistry, 5830 University Research Ct., College Park, MD 20740.
E-mail: pius.lee@noaa.gov

DOI: 10.1175/WAF-D-15-0163.1

TABLE 1. Schematic contingency table for an exceedance forecast with N data points.

	Observed	Not observed	Total
Forecasted	a	b	$a + b$
Not forecasted	c	d	$c + d$
Total	$a + c$	$b + d$	Sample size: $N = a + b + c + d$

guidance for the nation has been issued since September 2007 (Stajner et al. 2012a) and developmental PM_{2.5} forecast guidance since September 2009 (Mathur et al. 2008).

The NOAA/Air Resources Laboratory (ARL) and the National Centers for Environmental Prediction (NCEP) develop upgrades for the NAQFC forecasting system, and conduct and evaluate pre-implementation testing. The NAQFC comprises an offline coupling of the North American Model (NAM) Nonhydrostatic Multiscale Model with Arakawa B-grid staggering (NMMB) and the Environmental Protection Agency's (EPA) Community Multiscale Air Quality Model (CMAQ). Surface O₃ concentration forecasts are issued out to 48 h twice daily for the 0600 and 1200 UTC cycles (Chai et al. 2013). Predictions for each cycle are available online (<http://airquality.weather.gov>) by 1300 and 1730 UTC. The accuracy criterion for a successful O₃ forecast was determined to be achieving at least a 0.9 value in fraction correct (FC), which is also referred to as proportion correct (Davidson 2009). FC is calculated as the ratio of the sum of correctly predicted exceedances and correctly predicted nonexceedances defined by the primary National Ambient Air Quality Standard (NAAQS) threshold for the maximum daily 8-h-averaged surface (MDA8) O₃ concentration to the total number of measurements. NAAQS for MDA8 was 75 ppbv between March 2008 and October 2015. The monitoring stations used for this accuracy criterion compose the EPA AIRNow surface monitoring network (EPA 2015a). These monitors provide real-time surface measurements of air pollutant concentrations collected using federal reference or equivalent methods operated by local environmental and state agencies. AIRNow collects hourly data from about 1300 O₃ reporting stations across the country between June and September and has done so since 2007. In total this network reports about 158 600 MDA8 ozone measurements from June to September. The number of O₃ concentration reporting stations in the AIRNow network decreases to about 1000 for the remaining months of the year. During the O₃ seasons between 2009 and 2014, the NAQFC O₃ forecast guidance exceeded FC of 0.90 or greater for each monthly average. Moreover, the daily FC exceeded 0.90 for all but 2, 5, 6, 8, 2, and 1 days for the 6 yr from 2009 to 2014, respectively (Stajner et al. 2012b, 2014).

Another popular performance measure is the Heidke skill score or the equitable threat score (ETS) defined using a 2×2 contingency table for an exceedance forecast (Table 1). In Table 1, a denotes the number of exceedances correctly forecasted, b represents the number of forecasted exceedances that were not observed (false alarms), c denotes the number of observed exceedances that were not forecasted, and d represents the number of correctly forecasted nonexceedances:

$$\text{ETS} = \frac{a - S_f}{a + b + c - S_f} \quad \text{and} \quad (1)$$

$$S_f = \left(\frac{a + c}{N} \right)^2, \quad (2)$$

where S_f is the probability of randomly predicting an exceedance based only on the climatological probability of exceedance [Eq. (2)]. ETS removes the effects of random chance (Gandin and Murphy 1992) while measuring the fraction of forecasts correctly predicted. The ETS can vary from negative to 0 for poor forecast performance and from 0 to 1, where the larger the value, the better the forecast. The ETS is likely to be a better measure than FC because it allows forecast performance to be evaluated accounting for both event and nonevent forecasts as well as excluding those successful forecasts that result from chance. The continental United States (CONUS) wide averaged ETS in percent (%) for the period between 1 June and 31 September for MDA8 for the years of 2009–14 are 16%, 16%, 19%, 20%, 16%, and 17%, respectively.

The NAAQS for MDA8 O₃ was set at 75 ppb in March 2008. It coincides with the category “code orange” threshold, beyond which adverse human health effects are expected for sensitive groups. It was strengthened from a previous threshold of 80 ppb that was promulgated in July 1997 and in effect until March 2008. In December 2014, the EPA proposed that this NAAQS was to be further tightened to lie between 65 and 70 ppb (EPA 2015b). On 1 October 2015, the EPA tightened the NAAQS to 70 ppb. This continued trend of tightening NAAQS reflects epidemiological evidence that impacts on human health are found at lower thresholds than those previously established (Tager et al. 2005). This trend poses considerable challenges for NAQFC in terms of its reduced margins

for allowable errors. Any proposed upgrade to the NAQFC operational forecast guidance should continue to match and supersede FC for operational ozone predictions and lead to the improvement of $\text{PM}_{2.5}$ predictions for all seasons.

Beginning in January 2015, the same NCEP model that produces operational O_3 forecast guidance is also producing developmental $\text{PM}_{2.5}$ forecast guidance. Between 2009 and 2014, the $\text{PM}_{2.5}$ developmental product was generated by a nonoperational version of the NAQFC system with results disseminated to select local and state air quality forecasters participating in the NAQFC Air Quality Forecaster Focus Group (AQFFG). The distinction between the operational and developmental modes of the NAQFC forecast guidance is based on how well they meet requirements for reliable on-time delivery, accuracy, and format compliance, as well as their respective content and scope of recipients for product dissemination. Operational products are guaranteed to be available and to be disseminated on time to the general public in graphical and World Meteorological Organization (WMO) standardized formatted files in links and data portals found online (<http://airquality.weather.gov/>).

By design, developmental product testing fosters a dialogue between forecast system developers and the AQFFG to accelerate the improvement of developmental forecasting products to satisfy the proposed success criteria. An FC of at least 0.9 is required for the 24-h-averaged forecast surface concentrations for $\text{PM}_{2.5}$ with respect to the primary NAAQS threshold of $35 \mu\text{g m}^{-3}$. This FC requirement for the forecast accuracy between 2010 and 2014 was not met. The FC has been evaluated against about 1000 hourly reporting monitoring stations in the AIRNow network. There was a seasonal pattern to the rather dismal performance by the developmental $\text{PM}_{2.5}$ forecast. There was significant underprediction in summer and overprediction in winter. During the five years between 2010 and 2014, the averaged FC for the developmental $\text{PM}_{2.5}$ forecast did not improved much over time. It averaged between 0.67 and 0.74 over the summer months of June–September and between 0.58 and 0.64 over the winter months of November–February. In [appendix A \(Fig. A1\)](#), we illustrate this verification calculation for the ETS criterion across the period for the thresholds between 0.5 and $35 \mu\text{g m}^{-3}$. Again, the ETS skill did not improve noticeably over time especially for the high thresholds.

This paper overviews the current NAQFC system and performance for O_3 and $\text{PM}_{2.5}$. The following section provides the model description. [Section 3](#) focuses on the CMAQ components of the NAQFC

system, and [section 4](#) provides sensitivity analyses and evaluations. Results and discussion are presented in the final section.

2. Model description

[Figure 1](#) shows the schematic of the developmental NAQFC modeling system for the forecasting of surface $\text{PM}_{2.5}$ concentrations. It is a regional system comprising a numerical weather prediction (NWP) model and a chemical transport model (CTM) coupled together in an offline arrangement where the NWP model provides predicted meteorological fields to the CTM at hourly intervals. The NWP model is the NOAA/National Weather Service's (NWS) NAM. NAM is based on the aforementioned NMMB ([Janjić and Gall 2012](#)). NAM provides operational weather predictions for the United States out to 84 h based on a 12-km horizontal grid. The NAM domain covers nearly one-third of the Northern Hemisphere, spanning from near the equator to the North Pole from south to north and with its southwestern corner at around 1000 km southwest of the Hawaiian Islands and its northeastern corner in northern Europe in a rotated latitude–longitudinal map projection ([Fig. 2](#)). Although the meteorology is available for all 50 states, the developmental $\text{PM}_{2.5}$ product began with coverage for the CONUS in 2009 and was expanded to cover Alaska and Hawaii by 2010. A modified version of the EPA's CMAQ model version 4.6, dubbed CMAQv4.6.5, is the CTM in this system ([Fig. 1](#)). CMAQ is also run with 12-km horizontal grid spacing, but with a Lambert conformal conic (LCC) map projection. The offline coupling between NAM and CMAQ is achieved by two pre-processors: (i) Prdgen, which handles the horizontal map projection transformation for the meteorological variables from the NMMB grid to the CMAQ LCC grid through the NCEP IPOLATES code, a geometric interpolation package; and (ii) Premaq, which handles grid-staggering transformation, meteorological modulation of emission fluxes, and the collapse of the vertical grid structure from NMMB's 60 hybrid sigma–pressure layers to CMAQ's 22 sigma–pressure (σ – p) layers using a pressure–surface–based linear interpolation between the two NAM levels containing a CMAQ layer. These interface processors are described in further detail in [sections 2b](#) and [2c](#), respectively. In addition to the coupled NMMB–CMAQ system, there are other components such as the emission module and the chemical lateral boundary condition builder as well as the product generating postprocessing components. The emission module is described in [section 2d](#). Handling of boundary conditions

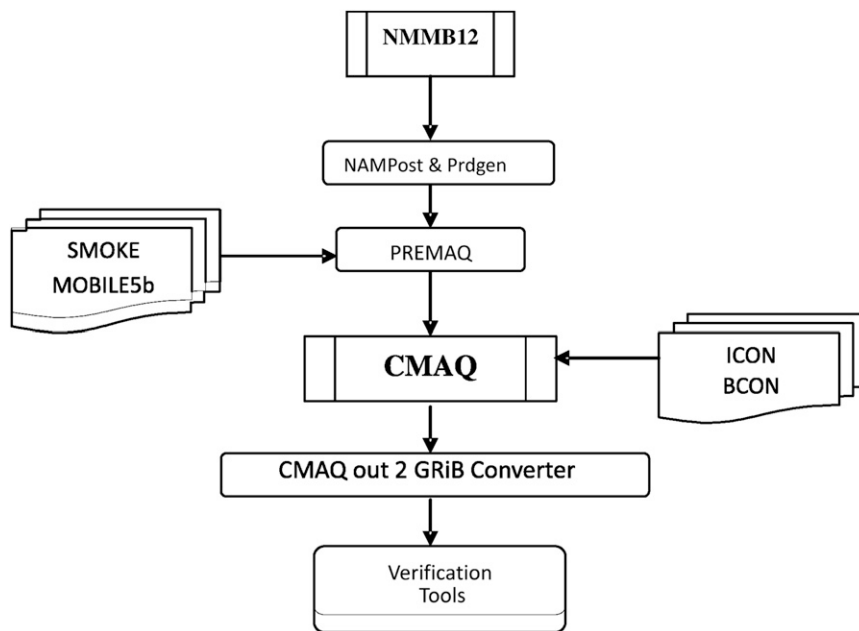


FIG. 1. Schematic of the developmental NAQFC $PM_{2.5}$ forecasting system: NMMB12 is the NWS mesoscale meteorological model, NAMpost calculates prognostic and diagnostic fields from NMMB12, Prdgen interpolates those meteorological fields from the NAM native grid onto an LCC grid, PREMAQ reads the LCC-grid-projected fields for CMAQ as well as prepares for CMAQ emission and process rate files by using preprocessors SMOKE and MOBILE5b, and CMAQ is the chemical transport model that reads the ICON and BCON respective outputs for initial and chemical boundary conditions. CMAQ with PREMAQ simulates air quality to generate O_3 and $PM_{2.5}$ surface concentration forecasts. The GRIB converter and verification tools postprocess and evaluate the forecast.

is described as part of the description for the CTM in section 3.

a. NAM configuration

The NWS regional NAM meteorological model is based on the NMMB (Janjić and Gall 2012), covering all 50 states and territories of the United States since October 2011. The physics packages are similar to those of its predecessors: the NCEP Eta Model that was retired from operation in October 2006, and the NCEP WRF-NMM model, retired in October 2011 (Table 2). These three generations of NAM used a rotated latitude–longitude map projection (Janjić et al. 2001). Regional data assimilation systems are used to assimilate meteorological and land surface observational data and provide initial conditions: NAM Data Assimilation System (NDAS) (Wu et al. 2002), and the Noah land surface model (LSM) based Data Assimilation System (NLDAS) provides land states (Mitchell et al. 2004). The advection time step for the 12-km NMMB is 26.7 s. Turbulence and moist processes are computed every 160 s. Both the horizontal and vertical advection schemes are positive definite and conservative for

total kinetic energy and hydrometeors. The vertical grid structure is an application of the general hybrid pressure–sigma and isobaric coordinate system after Eckermann (2009). There are 60 layers spanning the area between the surface and the model top at 2 hPa. The vertical grid spacing is more refined near the surface and around the most probable heights of a fully developed summer planetary boundary layer (PBL) top and of a midlatitude spring tropopause. NAM outputs hourly meteorological and hydrological fields at its native horizontal and vertical coordinates for CMAQ.

b. Processing of NMMB output using Prdgen

The NAM output for CMAQ consists of 3D and 2D fields (see Table B1). The Prdgen interface processor handles the variable horizontal map transform from the NAM grid to the CMAQ grid. Horizontal interpolation schemes are used to determine the so-called cross-point values of the resulting grid on the intermediate LCC projection with Arakawa A-grid staggering. Most variables use a bilinear algorithm applied to distance. The remaining variables that exhibit a stronger discrete

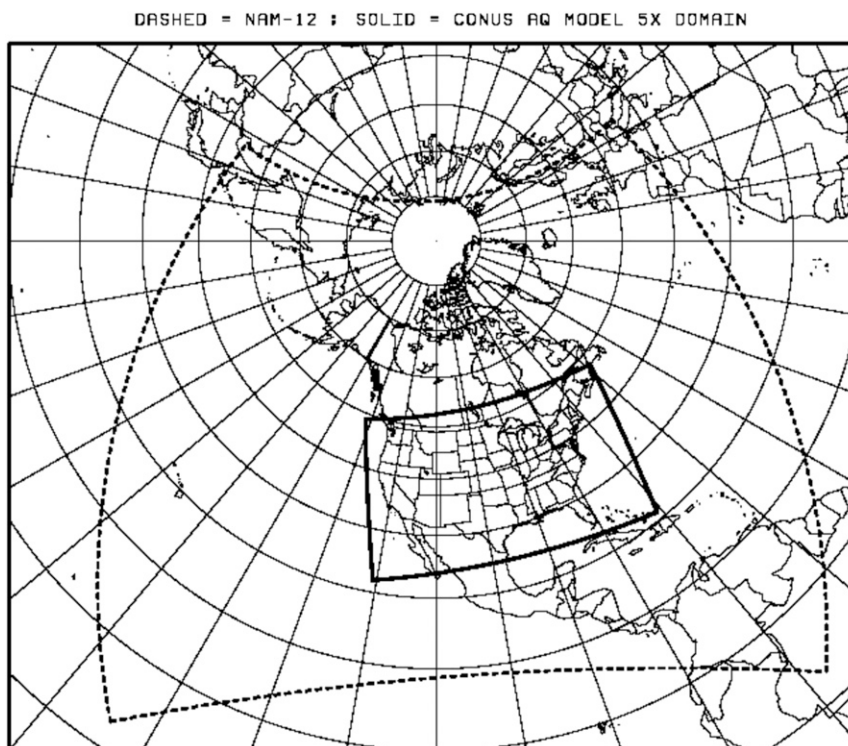


FIG. 2. The NCEP NAM (12 km) domain (outline shown by the dashed line). The NAQFC CONUS domain is also shown by the boldface frame.

characteristic use a nearest-neighbor algorithm to adopt the value pertaining to the closest cross point in the NAM grid.

c. Using Premaq to read Prdgen output fields and interpolate to CMAQ vertical levels

CMAQ uses an LCC map projection with Arakawa C-grid staggering. The second interface processor, Premaq, is invoked sequentially after the completion of Prdgen to complete the grid-staggering transformation (Fig. 1 and section 2b). Originally designed and implemented by Otte et al. (2005) for an initial version of

the NAQFC that provided surface O₃ forecasts for the northeastern United States, Premaq’s basic functionality of grid-staggering transformation and emission flux rate calculations remains valid, but has been substantially improved through a series of upgrades in NAM and CMAQ. A major NAM-related upgrade was the retirement of the Eta step-mountain vertical grid structure and the adoption of a hybrid isobaric and terrain-following vertical structure in NMMB. In addition, Premaq was also modified significantly to accommodate version upgrades in CMAQ that often entailed additional meteorological input. Premaq performs both

TABLE 2. Physics options in NMMB.

Process addressed	Scheme	Remarks and references
Horizontal advection	Adams–Bashforth	For basic dynamical variables and Coriolis force
Vertical advection	Crank–Nicholson	
Horizontal diffusion	Forward nonlinear	“Smagorinsky type” (Janjić 1990)
PBL	Mellor–Yamada–Janjić (MYJ)	Level 2.5 turbulence closure (Janjić et al. 2001)
Surface layer	Monin–Obukhov similarity	Accounting for viscous sublayer over water and land (Janjić 1994)
Radiation	Rapid Radiative Transfer Model (RRTM)	Mlawer et al. (1997)
Cumulus cloud	Betts–Miller–Janjić	Convective adjustment (Janjić 2000)
Cloud microphysics	Ferrier–Aligo	Aligo et al. (2014)
Surface exchanges	Noah land surface model	Ek et al. (2003)
Mountain blocking	Gravity wave drag	Alpert (2004)

TABLE 3. Typical dry deposition velocities predicted by the NAQFC.

Species	Predicted dry deposition velocity (cm s ⁻¹)
SO ₂	1–14
NO ₂	0.05–0.55
NH ₃	2–22
HONO	1–17
N ₂ O ₅	1–13
HNO ₃ and NO ₃ ⁻	1–16
PAN	0.1–1.5
O ₃	0.1–1.8
H ₂ O ₂	1–18
Aldehyde	0.2–3.8
HCHO	1–20
CO	0.01–0.14

the redistribution of the Prdgen processed fields in Arakawa A-grid staggering to C-grid staggering and a reduction of vertical levels from 60 to 22 to decrease the wall-clock time required for operational predictions.

Premaq also computes and outputs CMAQ-ready fields for dry deposition velocities, cloud-cover-induced photolytic rate attenuation coefficients, emission altitudes, and flux rates of air pollutants at each hour throughout a 48-h forecast. Premaq produces the same CMAQ-ready input files as the EPA's Meteorology–Chemistry Interface Processor (MCIP). [See Tables 2–4 in [Otte and Pleim \(2010\)](#).] Premaq adds a few more fields such as snow-cover and clear-sky downward shortwave solar flux to enhance the physics package consistencies between NAM and CMAQ.

The gaseous species dry depositional velocity calculation follows that of the “M3Dry” model in MCIP version 3.4.1 ([Otte and Pleim 2010](#)). NAM surface parameters such as canopy water and canopy conductance were provided by NAM to retain consistency between NMMB and CMAQ. [Table 3](#) shows typical values of the depositional velocities used in the NAQFC under ordinary ambient conditions. Satellite-retrieval-based canopy heights ([Lefsky 2010](#)) are included in the roughness length estimate for the aerodynamic resistance calculation. A multiplicative factor was employed to scale tree canopy height to roughness length for computing dry deposition velocities ([Brutsaert 1982](#)).

Photolytic rates are proportional to the ambient actinic flux. Above cloud enhanced photolytic rates due to reflection from clouds are accounted for in the standard releases of CMAQ ([Byun and Ching 1999](#)). The in situ photolytic rate attenuation coefficient equals unity at the cloud top. The in situ photolytic rate attenuation coefficient at each height at and below the cloud base is equal to the ratio of shortwave solar radiation reaching that height to the radiation that would reach that height under clear-sky conditions. Photolytic rates within the

TABLE 4. NAQFC emission categories using NEI2011, beginning 1 May 2015.

Category ^a	Description (unit)
ag	Agricultural NH ₃ sources (mol km ⁻² s ⁻¹)
c1c2rail	Class I and II water navigation and railroad emissions ^b (mol km ⁻¹ s ⁻¹)
othon	Mexican ^c and Canadian ^d mobile sources (mol km ⁻¹ s ⁻¹)
nonroad	Off-road engines (United States; mol km ⁻¹ s ⁻¹)
nonpt	Other U.S. area sources (mol km ⁻² s ⁻¹)
othar	Mexican ^c and Canadian ^d area sources (mol km ⁻² s ⁻¹)
np_oilgas	Nonpoint oil and gas sources (mol km ⁻² s ⁻¹)
rwc	Residential wood combustion (mol km ⁻² s ⁻¹)
othpt	Mexican ^c and Canadian ^d point sources (mol km ⁻² s ⁻¹)

^a Reference names are as in the EPA's Source Classification Code.

^b Inland water and coastal traffic not counting the ocean liners.

^c The 2012 Mexico NEI for Mexico.

^d The 2010 Environment Canada National Inventory for Canada.

cloud are interpolated between the cloud-top and cloud-base values using the in situ cloud cover fraction at that height.

To generate CMAQ-ready emission files for forecasting, Premaq provides emissions fluxes for point, area, and nonroad, mobile, and biogenic sources on the CMAQ grid. The following subsections elaborate on the methodology adopted to perform the various emission projections and modulations targeting a given forecasting year.

d. Emission projections

The EPA's National Emission Inventory (NEI) 2011 version 1 is being incorporated into Premaq's emission projection schemes. The incorporation is accomplished in two phases, as the second phase requires a coordinated upgrade of the CTM that computationally parallelizes many of the calculations for meteorological-dependent emission processes. [Table 4](#) describes the emission sectors in the first phase of incorporating NEI 2011 into the NAQFC modeling system that became effective on 1 May 2015.

1) POINT SOURCES

The 2005 NEI version 1 (NEI05v1) was used as a first estimate for electric generating unit (EGU) and non-EGU U.S. nitrogen oxides (NO_x) and sulfur dioxide (SO₂) point source strengths. These point sources were updated with the 2014 Continuous Emission Monitoring (CEM) dataset—a biennial database. EGU projections were computed using the ratios of the emission strengths for 2012–14 and then extrapolating to 2015. In addition,

the regionally based Annual Energy Outlook (AEO) SO₂ and NO_x 2015 emission projection factors from the Department of Energy were used. For offshore large point sources, the EPA's 2008 offshore emission inventory was used. The Environment Canada (EC) 2011 point source National Emission Inventory (EI) was used for Canada. In Mexico, the 2012 Mexico National EI, version 2.2, was used for the six states in northern Mexico bordering the United States, and the Mexico EI version 1 was used for the interior states. Plume rise calculations account for the effective injection heights of buoyant pollution plumes based on stack height, initial discharge characteristics of the plume, and surrounding meteorological stability conditions (Briggs 1972). The plume-rise equations were then delineated into unstable, neutral, and stable atmospheric conditions (Byun and Ching 1999).

2) AREA AND NONROAD SOURCES

Except for off-road sources, a combination of the EPA's 2011 version 1 (2011NEIv1) and 2005 NEIv1 was used. The delineation to which inventory should be used for a particular sector depended on whether its processing was compatible with CMAQv4.6.5. Results from 2011 NEI were used for all agricultural NH₃; railway and class 1 and class 2 marine emissions primarily representing non-ocean-going activities; vehicular refueling; oil and gas industry related emissions; and residential wood combustion. Also, U.S. off-road emissions in the 2005 NEIv1 were replaced with the 2011 inventories. These inventory data were processed using the EPA's Sparse Matrix Operator Kernel Emissions (SMOKE) modeling system to represent monthly, weekly, daily, and holiday/non-holiday variations specific for the forecast year. Emissions from wildfires, prescribed agricultural burns, and land-clearing fires based on climatology were removed from the area source emissions and replaced with dynamic fire emission modeling using a version of the U.S. Forest Service BlueSky smoke emission package (O'Neill et al. 2009) and the NOAA/NESDIS Hazard Mapping System (HMS) for fire locations and strength. In terms of procedure, we processed emission inventories by sectors, and for the fire sectors, we did not include prescribed burns and wildfires from the NEIs. The 2006 Environment Canada National Inventory (EC NI) area sources were used for Canada, and the 2012 Mexico NEI nonroad sources were used for Mexico.

3) MOBILE SOURCE EMISSIONS

To reflect recent changes in mobile source emissions, the EPA's Office of Transportation and Air Quality 2005 on-road emission inventory was adjusted to 2012 basing on the EPA Cross State Air Pollution Rule

(CSAPR; available online at <http://www.epa.gov/airtransport/CSAPR/>). Both 2005 NEIs and the CSAPR-projected emission inventories were based on the MOBILE6 model. The CSAPR projection considered possible emission changes caused by the existing and predicted emission control regulations finalized in early 2009. The methodology generated on-road mobile emissions and the time-activity pattern counts for monthly, weekday/weekend, and diurnal variability for different vehicle types over the CONUS based on the EPA's emission factor model MOBILE6 (Tong et al. 2015b). The trends for NO_x emissions over large U.S. urban centers between 2005 and 2012 were analyzed using surface measurements based on the EPA Air Quality System (AQS).

The collocated column-integrated retrievals made by the Ozone Monitoring Instrument (OMI) on board the National Aeronautics and Space Administration (NASA) *Aura* spacecraft were well corroborated with the surface-based AQS data. OMI analyses yielded a 40% decrease over the period between 2005 and 2012 for the urban centers where NO_x emissions from vehicular activity were the dominant NO_x source sector (Tong et al. 2015b). We used the 2006 EC NI for Canada, and the 2012 Mexico NEI version inventory for Mexico.

4) BIOGENIC SOURCES

All inputs used in the forecast system were updated to the Biogenic Emission Inventory System (BEIS3), version 3.14. Biogenic emissions were calculated dynamically using the BEIS3 version 3.14, which considered variability in temperature and solar radiation to estimate NO and volatile organic compound (VOC) emissions from forests, grasslands, and croplands.

5) SEA SALT EMISSIONS

Sea salt can represent a significant mass percentage of the aerosol concentration in coastal areas. Sea salt emissions were parameterized as a function of 10-m wind speed and surf zone category. In open oceans, sea spray is the dominant emission mechanism. In the surf zone, wave breaking contributes a larger amount of sea salt emission than in the open oceans. CMAQ v4.6.5 does not use any heterogeneous chemical or depositional processes for sea salt. Sea salt is treated as an inert species in coarse and accumulation modes. Emissions of trace gases and organic aerosols from the ocean have not been included in the NAQFC system.

6) SUPPRESSION OF FUGITIVE DUST BY ICE AND SNOW COVER

Fugitive dust, a significant component of PM_{2.5}, is predominantly composed of mineral and crustal elements and compounds. CONUS-wide average fugitive

dust emission sources from paved and unpaved roads account for approximately 7% and 46% of the total fugitive dust emission, respectively. Both sources have crustal and organic carbon components as their major mass fractions. For paved road sources, 89% and 10% of the emissions in this sector are attributed to the crustal and organic carbon components, respectively. For unpaved roads the attributions are approximately 94% and 6%, respectively. Other significant sources included airstrips, construction sites, and fields undergoing tilling and harvesting. These sources do not apply when the surface is covered by ice or snow. NAM-predicted snow cover fraction is used to scale the emissions fluxes.

7) INTERMITTENT EMISSIONS FROM FIRE AND DUST

Windblown dust storms and wildland fires contribute a large amount of fine particulates to the surface. Premaq deals with both of these intermittent emission sources originating in the CONUS domain. Premaq provides CMAQ with a 3D emissions file for these intermittent sources.

The HMS was used to provide fire-point and smoke-plume locations by blending multiple satellite retrievals with human analyst products (Ruminski et al. 2006). The U.S. Forest Service BlueSky smoke emission package (O'Neill et al. 2009; Larkin et al. 2009) was used with HMS to estimate near-real-time smoke emissions. Wildfires that were estimated to last at least 24 h were used as emission sources into the NAQFC. BlueSky provides emissions of PM_{2.5}, particulate matter smaller than 10 μm in diameter (PM₁₀), carbon monoxide (CO), carbon dioxide (CO₂), methane (CH₄) and VOCs from wildfires. Emission rates of others species contributing to the chemical mechanisms in CMAQ, such as elemental carbon (EC), black carbon (BC), nitrogen oxides (NO_x), VOCs, ammonia (NH₃), and sulfur dioxide (SO₂) were estimated by scaling them to that of CO, a wildfire signature species, using their mass ratios with CO (Hsu and Divita 2011). The BlueSky wildfire heat flux was also estimated and used in the Briggs equation (Briggs 1972), to determine injection heights.

Lifting of crustal and mineral elements by winds constitutes a major intermittent primary particulate matter source over barren land, dry river beds, and large swathes of arid land in the United States. The topography, soil surface water content, and textural characteristics are among the governing factors for crustal particle uplift and suspension. Wind gusts surpassing a certain threshold specific to those characteristics will dislodge the particles. Turbulence and wind shear within the boundary layer keep the particle airborne and may bring it to a higher altitude. Tong et al. (2015a) followed and

modified the methodology presented by Owen (1964) to determine the instantaneous lifting rates. The large range of parameters in Owen's model and the non-erodible and moistened effects of the topsoil result in significant uncertainties for modeled soil particle lifting rates. The developmental NAQFC system also includes the effects of rain and snow on erodible topsoil elements (Tong et al. 2015a). Forecast results and verification from the modeling system for a dust storm active season are shown in section 4.

3. NAQFC CMAQv4.6.5

a. Transport

CMAQ integrates the species continuity equation in a generalized curvilinear coordinate system (Byun and Schere 2006):

$$\frac{\partial(\phi_i J_s)}{\partial t} + m^2 \nabla_s \cdot \left(\frac{\phi_i J_s \hat{\mathbf{V}}_s}{m^2} \right) + \frac{\partial(\phi_i J_s \hat{v}^3)}{\partial s} = J_s, \quad (3)$$

where ϕ_i is the concentration of i th advected species (in kg m^{-3}), with $i = (1, 2, \dots, 130)$ for CMAQ v4.6.5, a NAQFC customized CMAQ model version based on CMAQ version 4.6; $J_s = |\partial z / \partial s|$ is the vertical Jacobian of the terrain-influenced general vertical coordinate s ; $z(\hat{x}^1, \hat{x}^2, \hat{x}^3, \hat{t}) = h_{\text{AGL}}(\hat{x}^1, \hat{x}^2, \hat{x}^3, \hat{t}) + z_{\text{sfc}}(\hat{x}^1, \hat{x}^2)$, z is the geometric height, h_{AGL} is the height above ground level (AGL), and z_{sfc} represents the topographical height. The generalized curvilinear coordinates $(\hat{x}^1, \hat{x}^2, \hat{x}^3, \hat{t})$ are related to the reference rotated earth-tangential coordinates (x, y, z, t) . In addition, $\nabla_s = \partial / \partial \hat{x}^1 \hat{\mathbf{i}} + \partial / \partial \hat{x}^2 \hat{\mathbf{j}}$ is a divergence operator and $\hat{\mathbf{V}}_s = \hat{v}^1 \hat{\mathbf{i}} + \hat{v}^2 \hat{\mathbf{j}}$. Furthermore, \hat{v}^1 , \hat{v}^2 , and \hat{v}^3 are the contravariant wind components in generalized curvilinear coordinates. The quantity Q_{ϕ_i} represents the loss and production terms of the species, including chemical reactions, and physical processes such as deposition and emission fluxes. CMAQ assumes $\hat{v}^3 = 0$ at the model top; thus, there is no mass exchange by vertical advection at the model top. It also adopts a zero-flux condition from concentration gradients at the model top (Byun and Ching 1999).

Advection is implemented using the piecewise parabolic method (PPM) advection scheme (Collela and Woodward 1984; Byun and Schere 2006). For convective mixing, a combined local and nonlocal mixing closure model [Asymmetric Convective Model 2 (ACM2)] is used to vertically distribute trace gases and aerosols. Mass is entrained through a gradual layer-by-layer compensatory subsidence in ACM2 (Pleim 2007a,b). ACM2 is used for small-scale eddies and large-scale turbulent mixing in the boundary layer. In non- or

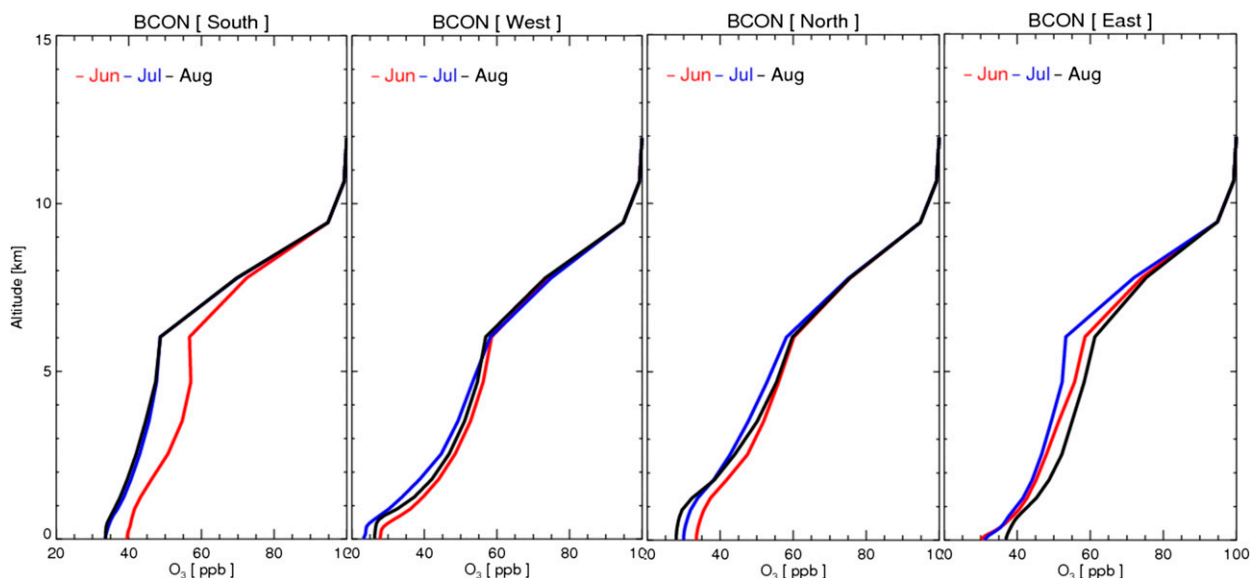


FIG. 3. Monthly varying lateral boundary conditions for the NAQFC CONUS domain for O_3 (ppb) for June (red), July (blue), and August (black) averaged at the (a) south, (b) west (c) north, and (d) east lateral boundaries.

weakly convective conditions the ACM2 scheme simulates the suppressed mixing accurately. Some studies utilizing the NAM output vertical eddy diffusivity and the diffusion equation directly for simulating turbulent mixing in the stable boundary layer have shown promising results comparable with those from ACM2 (Lee et al. 2009).

b. Boundary conditions

At the lateral boundaries, with \mathbf{n} denoting the outward normal vector, $\hat{\mathbf{V}}_s \cdot \mathbf{n} \leq 0$ specifying an inflow condition and $\hat{\mathbf{V}}_s \cdot \mathbf{n} > 0$ an outflow condition, respectively. A zero-flux divergence outflow condition is imposed (Byun and Schere 2006). For the inflow conditions, concentrations are set at the lateral boundaries by prescribed values. We adopted a species mapping methodology between the GEOS-Chem global chemical transport model and CMAQ (Tang et al. 2009). Monthly averaged concentrations for 36 gaseous and aerosol species obtained from a GEOS-Chem simulation for the year 2006 were used as lateral boundary conditions (LBCs) below 7-km altitude (Tang et al. 2009; Bey et al. 2001). A “clean-air scenario” static condition was used between 7 km and model top. Figures 3a–d show the monthly averaged LBCs for O_3 for June–August averaged over the NAQFC CONUS domain boundaries.

c. Model options

Table 5 summarizes the CMAQ model options selected for the various geometric configurations and

physical and chemical schemes. The 22 σ - p terrain-following layers represent the atmospheric column between the surface and the model top at 100 hPa, with the first 14 layers covering the lowest 2 km, which is critical for both the meteorological and air quality models (Lee and Ngan 2011). The geometric thickness of layers is the thinnest near the surface and increases unevenly with altitude. The top of the lowest model layer is at 39 m AGL.

The interested reader is referred to “The CMAQ Science Algorithm” by Byun and Ching (1999) and subsequent EPA technical reports (e.g., Edney et al. 2007), as well as the MODELS3 website CMAQ Release Notes in Community Modeling and Analysis System (CMAS), for details concerning the parameterization of the physical and chemical processes.

d. Model modifications

Several modifications to CMAQ version 4.6 were made to improve the consistency of the physics package between NAM and CMAQ. In section 2c, we already described the modifications for consistency used in Premaq. Removal of gas constituents by dry deposition in the CMAQ model is calculated by multiplying their respective surface level concentrations with deposition velocities (Pleim et al. 1997; Binkowski and Shankar 1995). The deposition velocities for gaseous species utilize the resistance approach analogous to Ohm’s law in electrical circuits. For aqueous-phase chemistry and in- and below-cloud scavenging, the cloud liquid water content is diagnosed from cloud top

TABLE 5. CMAQ4.6.5 physics and chemistry options for the PM_{2.5} developmental forecast.

	Scheme and configuration	Remarks and references
Map projection	LCC	Byun and Ching (1999)
Vertical layers	22 σ -p layers with lowest 14 within 2 km from the surface; CMAQ model top at 100 hPa	
Horizontal and vertical advection	PPM	Colella and Woodward (1984)
Horizontal diffusion	Eddy diffusivity theory	Pasquill and Smith (1983)
Vertical diffusion	K theory	Byun and Dennis (1995)
Convective mixing	ACM2	Pleim (2007a,b)
Gas mechanism	CB05	Yarwood et al. (2005)
Aerosol chemistry	Aero4	Binkowski and Roselle (2003)
Anthropogenic emission	NEI2011 (Table 3)	EPA (2015b)
Biogenic emission	BEIS3.14	Schwede et al. 2005
Chemical LBC	Monthly avg imposed on static LBCs (section 3)	

and base, and from the predicted rate of convective precipitation.

Additional modifications of the standard CMAQ include the following: 1) faster removal of organic nitrate (NTR) and reduction in its sequestration efficiencies within the Carbon-Bond 2005 (CB05) gas-phase mechanism by increasing the photolysis frequency by a factor of 10 (Saylor and Stein 2012; Canty et al. 2015); this modification typically shortens the predicted lifetime of NTR in CMAQ from about a week to approximately a day (Pan et al. 2014); and 2) a minimum PBL height of 50 m avoids total suppression of vertical diffusive mixing.

e. Aerosol processes

The NAQFC CMAQ v4.6.5 follows largely the EPA's Aero4 module and the related emission and removal processes found in CMAQ version 4.6. Gas-to-particle conversion, heterogeneous reactions, depositional growth, and coagulation are included (Edney et al. 2007; Carlton et al. 2008; Kelly et al. 2009). The Aero4 module simulates particle formation, condensational and coagulation growth, or evaporative dissipation of existing particles due to ambient chemical, temperature, and humidity conditions. The removal processes are modeled outside Aero4 in the cloud, scavenging, and dry deposition modules. The aerosol processes and their parameterizations pertinent to Aero4 have been described in details by Byun and Schere (2006) and Binkowski and Roselle (2003). Two major modifications from CMAQ 4.6 were adopted for emissions: 1) modulation of fugitive dust emission due to snow and ice cover [see section 2d(6)] and 2) the inclusion of windblown dust [see section 2d(7)].

Aero4 adopts a modal approach to categorize particulate matter by its diameter prescribed as lognormal distributions into two fine modes: the Aitken mode with diameters peaking between 0.01 and 0.1 μm , and an accumulation mode with diameters peaking between 0.1 and 1.0 μm . In addition, a coarse mode is also

represented by a lognormal size distribution with diameters peaking between 1.0 and 10.0 μm .

Fine particles in CMAQ often reflect fresh emissions of elemental carbon from incomplete combustion or from new particle formation through binary homogeneous nucleation of sulfuric acid vapor with water vapor. The nighttime heterogeneous conversion of N₂O₅ to nitric acid can also be a significant pathway for fine particle formation and growth, especially under warm and humid conditions (Bhave et al. 2006). Condensation of semi-volatile carbonaceous compounds from anthropogenic and biogenic sources such as alkanes, aromatics, terpenes, and other VOCs can condense to form secondary aerosols. Coarse mode particles emerge predominantly from emissions related to dislodgements of crustal mineral aerosols by wind, vehicular and agricultural activities, and maritime aerosols such as sea salt from sea spray in the surf zone. Once a fine particle is formed, Aero4's ISORROPIA (Nenes et al. 1998), a thermodynamic equilibrium model, determines the partition between the gas and the particulate phases of ammonia, nitrate, sulfate, and water species.

Dry deposition velocities for particles are parameterized by size-dependent sedimentation (Binkowski and Shankar 1995). CMAQ treats pollutants differently for in- and below-cloud scavenging depending on whether a pollutant participates in the aqueous-phase reactions. The accumulation and coarse mode particles are assumed to be completely absorbed by the cloud and rainwater whereas the Aitken mode particles are treated as interstitial aerosols. An Aitken mode particle can coagulate with other particles or be absorbed by a cloud or rain droplet. An absorbed particle can reemerge as a dry particle by resuspension and evaporation.

The aerosol mass wet removal rates depend proportionally on the rate of precipitation. Wet deposition trace species removal consists of in-cloud- and below-cloud scavenging and washout (Binkowski and Shankar

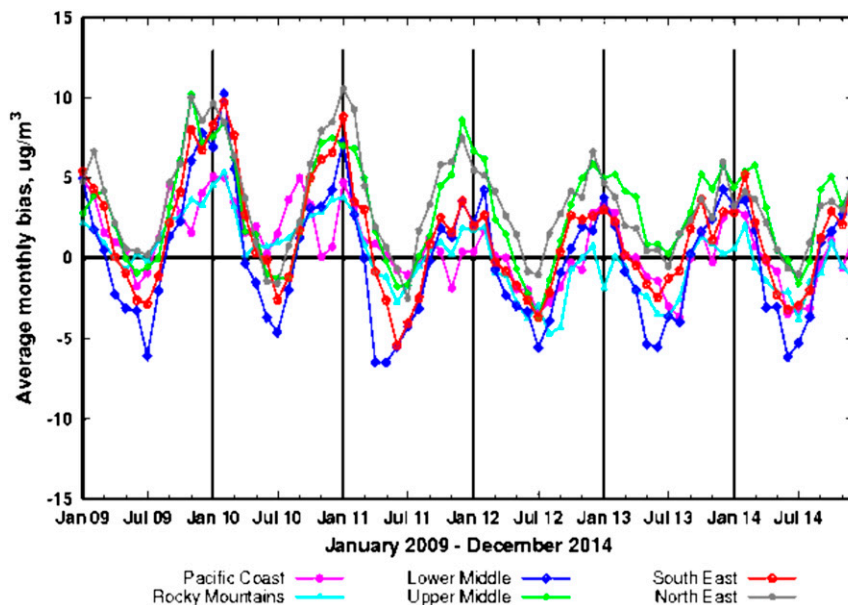


FIG. 4. Time series of regionally and monthly averaged biases for surface hourly $\text{PM}_{2.5}$ concentrations ($\mu\text{g m}^{-3}$) for the 2014- $\text{PM}_{2.5}$ forecast guidance between January 2009 and December 2014 (see Table 6) verified against the AIRNow network observations: PC (pink); LM (blue); SE (red); RM (cyan); UM (green); and NE (gray); with an average of 105, 60, 80, 50, 95, and 85 reporting stations over the period, respectively (Insets in Figs. 6 and 7 show the regional definitions.).

1995). NMMB-modeled hydrometeor fields were not used for wet deposition removal rate calculations in the NAQFC CMAQ. Diagnosed precipitation rates based on a diagnostic cloud volume reconstructed by the relative humidity profile given by NMMB were used instead (Chang et al. 1987).

4. Sensitivity analysis and evaluations

Developmental $\text{PM}_{2.5}$ forecast guidance was upgraded in January 2015. Three changes were made from the 2014 developmental $\text{PM}_{2.5}$ model: 1) intermittent emissions due to windblown dust originating inside the CONUS [section 2d(7)] and wildfires [section 2d(7)], 2) suppression of fugitive dust emissions by snow and ice cover [section 2d(6)], and 3) an accelerated removal of the organic nitrate (NTR) species (section 3).

To quantify the performance improvement from these upgrades (e.g., Fig. 4), we conducted several reforecast sensitivity studies across multiple seasons (Table 6). Experiment 2014- $\text{PM}_{2.5}$ refers to the configuration before the NCEP upgrade in January 2015, which had been the mainstay for our studying the forecast performance for surface $\text{PM}_{2.5}$ concentration. Figure 4 shows that between January 2009 and December 2014 wintertime overestimates had gradually been reduced as a result

of a reduction in the overestimation of mobile NO_x , resulting in reduced particulate NO_3^- . Experiment 2015- $\text{PM}_{2.5}$ represents the model configuration since the January 2015 upgrade, together with May 2015 emissions updates described in sections 2d(1)–2d(4) using a partial update from NEI2005 to NEI2011, as explained in Table 4. These emission updates are applied retroactively to all months in 2015 in the experiment 2015- $\text{PM}_{2.5}$ presented here. The No Dust experiment denotes the 2015- $\text{PM}_{2.5}$ configuration without real-time wind-blown dust emissions [see section 2d(7)]. Similarly, the No Wildfire, No Snow/Ice, and No J_{NTR}^* 10 cases denote the 2015- $\text{PM}_{2.5}$ configurations without the wildfire emission in section 2d(7), snow and ice cover suppression of fugitive dust in section 2d(6), and the increased photolysis frequency for NTR in section 3, respectively. All experiments in Table 6 were initialized once per day at 1200 UTC, except for the 2014- $\text{PM}_{2.5}$ configuration, where the model was initialized four times per day at 0000, 0600, 1200, and 1800 UTC. Only the prediction results from the 1200 UTC cycle run were used for evaluation. The last four experiments in Table 6 were performed for the season when they were expected to have the largest impact: dust events in late spring in the southern plains and in California, increases in the occurrence of wildfire and photolysis frequencies of carbonyl nitrates in midsummer, and wintertime suppression of

TABLE 6. Sensitivity runs.

Case name	Description	Period
2014-PM _{2.5}	Pre-developmental testing with NEI2005-based emissions	2009–14
2015-PM _{2.5}	NEI2011 according to Table 3; real-time dust emissions model; real-time wildfire; J_{NTR}^* 10, i.e., increase photolysis frequencies of carbonyl nitrates by a factor of 10; and suppression of fugitive dust emission when ice/snow is present	Since 1 May 2015
No Dust	2015-PM _{2.5} without dust	May 2014
No J_{NTR}^* 10	2015-PM _{2.5} without J_{NTR}^* 10	Jul 2014
No Wildfire	2015-PM _{2.5} without wildfire	Jul 2014
No Snow/Ice	2015-PM _{2.5} without suppression of fugitive dust emission when ice/snow present	Jan 2015

emissions of fugitive dust during periods of snow and/or ice cover. Figure 5 shows the diurnal cycle of PM_{2.5} biases for the 2014-PM_{2.5} and the 2015-PM_{2.5} configurations averaged over July 2014. A consistent improvement of 2015-PM_{2.5} forecasts over that of the 2014-PM_{2.5} simulation is seen.

Table 7 shows a few of the commonly used statistical measures for evaluating the various model predictions. The inclusion of intermittent emissions shows little impact. Across the CONUS, the normalized mean error (NME) was reduced from -21% to -20%, and from 29% to 28%, respectively, when the intermittent sources of windblown dust in May 2014 and inside-domain wildfires in July 2014 were included in the forecasting simulation.

Suppression of fugitive dust emission during winter conditions with snow and/or ice cover led to a considerable

improvement of the PM_{2.5} forecasts, as illustrated by the January 2015 results. Suppression of fugitive dust emissions by snow–ice cover during the period reduced the NME from 31% to 13% over CONUS. (Table 7). The ETS skill achieved by this treatment of suppressing the emission of fugitive dust reflected a threefold improvement.

Small impacts of NTR and wildfire treatments were observed for the Pacific coast (PC) region, but windblown dust treatment improves the PM_{2.5} representation for the Rocky Mountain (RM) region (Figs. 6 and 7). The abbreviations for the other four regions are as follows: UM, Upper Middle; LM, Lower Middle; NE, Northeast; and SE, Southeast of the CONUS.

Table 7 shows forecast guidance performance statistics for hourly averaged surface PM_{2.5} for May 2014 in

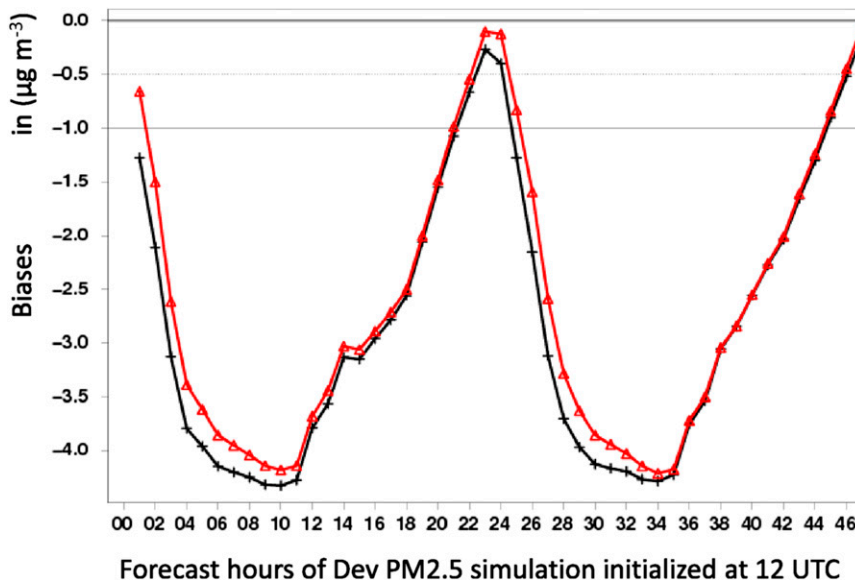


FIG. 5. Monthly CONUS-wide averaged hourly biases of predicted surface PM_{2.5} ($\mu\text{g m}^{-3}$) from the 1200 UTC cycle of the 2015-PM_{2.5} simulation for July 2014 for black showing 2014-PM_{2.5} and red showing 2015-PM_{2.5} forecasts, verified against the AIRNow surface network with about 510 reporting stations.

TABLE 7. Daily averaged surface PM_{2.5} forecast guidance performance statistics.

Case		Mean	Bias ($\mu\text{g m}^{-3}$)	NME (%)	RMSE	Corr coef r	ETS w.r.t. $35 \mu\text{g m}^{-3}$ (%)	
CONUS	May 2014 (dataset size = 3606)	Obs	7.76					
		2015-PM _{2.5}	6.20	-1.56	-20	4.46	0.32	-0.1
		No Dust	6.15	-1.61	-21	4.48	0.30	-0.1
	Jul 2014 (dataset size = 3594)	2014-PM _{2.5}	5.06	-2.70	-35	6.49	0.33	-0.2
		Obs	9.33					
		2015-PM _{2.5}	6.62	-2.71	-28	5.36	0.23	0.1
	Jan 2015 (dataset size = 3533)	No Wildfire	6.60	-2.73	-29	5.37	0.23	0.1
		2014-PM _{2.5}	6.85	-2.48	-27	8.84	0.22	0.06
		Obs	9.83					
Jan 2015 (dataset size = 3533)	2015-PM _{2.5}	11.16	1.33	13	6.46	0.38	0.8	
	No Snow/Ice	12.83	3.00	31	7.28	0.37	0.3	
	2014-PM _{2.5}	13.57	3.74	38	12.56	0.38	0.2	
RM	May 2014 (dataset size = 731)	Obs	6.68					
		2015-PM _{2.5}	4.40	-2.28	-34	7.68	0.27	0.0
		No Dust	4.14	-2.54	-38	8.01	0.12	0.0
		2014-PM _{2.5}	3.66	-3.02	-45	5.02	0.21	-0.03
PC	Jul 2014 (dataset size = 816)	Obs	7.95					
		2015-PM _{2.5}	4.46	-3.49	-44	8.43	0.19	-0.01
		No Wildfire	4.39	-3.56	-45	8.51	0.17	-0.01
		2014-PM _{2.5}	4.93	-3.02	-38	8.38	0.18	0.0
SE	Jul 2014 (dataset size = 523)	Obs	10.52					
		2015-PM _{2.5}	8.15	-2.37	-22	7.74	0.21	-0.2
		No J_{NTR}^* 10	8.15	-2.37	-22	7.74	0.21	-0.2
		2014-PM _{2.5}	7.91	-2.61	-25	7.70	0.22	-0.2
UM	Jan 2015 (dataset size = 650)	Obs	9.42					
		2015-PM _{2.5}	12.52	3.10	33	8.94	0.46	0.9
		No Snow/Ice	15.93	6.51	69	11.70	0.48	0.3
		2014-PM _{2.5}	12.87	3.45	37	9.12	0.46	0.2

RM, for July 2014 in PC, and for January 2015 in UM. During July 2014 there were numerous wildfires, especially in the western states. The northern and central Washington State wildfires beginning on 8 July 2014 caused significant damage to more than 1400 km². Southern California, the southern parts of Arizona, and

New Mexico also experienced more frequent wildfires with larger burnt areas than in an average year. The bias for PM_{2.5} in PC showed a small reduction from 3.56 to 3.49 $\mu\text{g m}^{-3}$, in a regional-wide observation of 7.95 $\mu\text{g m}^{-3}$, and an improved r , from 0.17 to 0.19, when wildfire emissions were included in the model

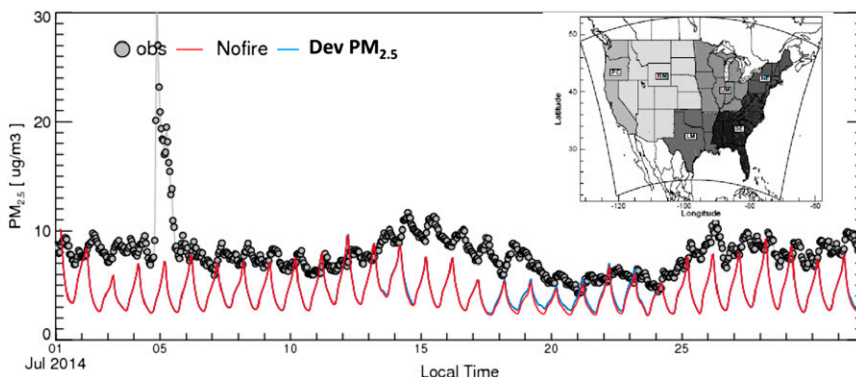


FIG. 6. The PM_{2.5} observed (gray circles) and predicted concentrations ($\mu\text{g m}^{-3}$) for the PC region (depicted in the inset) averaged over 117 AIRNow stations during July 2014 for the 2015-PM_{2.5} developmental NAQFC PM_{2.5} forecast guidance (blue), and the No NTR and No Wildfire (red) experiments.

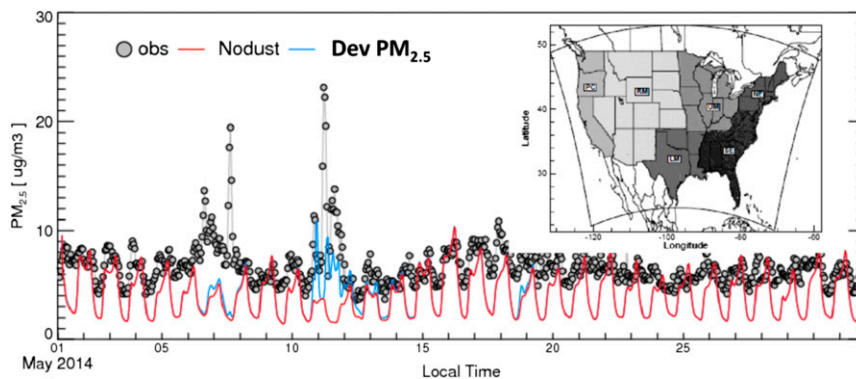


FIG. 7. As in Fig. 6, but for the RM region averaged over 57 AIRNow stations during May 2014 for NAQFC $PM_{2.5}$ forecast guidance and the No Dust experiment.

(Fig. 6). The change in the photolysis frequencies for the NTR compounds where there was an abundance of volatile organic compound in relation to that of NO_x was also examined for the July 2014 case. The impact was primarily on the gaseous species and secondarily on $PM_{2.5}$. The largest impact of the NTR change was seen in the SE region where the MDA8 O_3 bias was reduced from 8.1 to 7.9 ppbv, a 3% improvement; and the root-mean-square error (RMSE) was reduced slightly from 13.54 to 13.44 ppbv. This was due to the exacerbated overpredictions in rural areas, which nearly offset urban area improvements in the regional-scale evaluation. The shortened life of NTR in urban areas resulted in faster transformation into peroxyacyl nitrates (PAN) and affected photochemical reactions in the downwind rural areas, typically resulting in higher O_3 production.

The May 2014 case was chosen to evaluate the impacts of windblown dust emissions due to a high frequency of dust storms in the western states. For instance, on 11 May 2014 multiple windblown dust storms occurred in Southern California, Nevada, Arizona, and Texas. The efficacy in capturing windblown emissions resulted in a considerable improvement in the $PM_{2.5}$ forecast. The correlation coefficient r for RM increased substantially from 0.12 to 0.27 when the windblown fugitive dust emissions were included (Fig. 7). Table 7 shows correspondingly noticeable improvement in NME, RMSE, and ETS skills by incorporating windblown dust emissions.

The January 2015 experiments evaluated the impact of the suppression of fugitive dust emission due to snow and ice cover. This suppression has the largest positive impact of all the sensitivity cases considered in this study. The bias in UM for the 24-h-averaged daily maximum $PM_{2.5}$ was reduced from 6.5 to 3.1 $\mu g m^{-3}$, which is a 52% improvement (Fig. 8).

5. Conclusions and discussion

In January 2015, NOAA/NWS/NCEP began providing the NAQFC developmental $PM_{2.5}$ forecast guidance, 2015- $PM_{2.5}$, using the same modeling system that generates the NAQFC operational O_3 forecast guidance. This developmental $PM_{2.5}$ forecast guidance and its predecessor, 2014- $PM_{2.5}$, have been disseminated to a select group of air quality forecasters from local and state environmental agencies in the NAQFC Air Quality Forecast Focus Group (AQFFG) for early use and evaluation beginning in 2009. Four major upgrades were included in 2015- $PM_{2.5}$: 1) incorporation of the base emission inventory from the EPA's 2011 National Emission Inventory (NEI), except for ocean-going ships and on-road mobile 2) incorporation of intermittent emission sources within the NAQFC domain accounting for wildfire emission projections and windblown dust emissions; 3) suppression of fugitive dust emissions when there is snow or ice covering the ground; and 4) increase of photolysis frequency of alkyl nitrate by one order of magnitude to shorten the lifetime of organic nitrate in the gaseous mechanism. These modifications improved both the $PM_{2.5}$ and O_3 forecasts as demonstrated by verification against observations from the EPA's AIRNow surface monitoring network. Four sensitivity studies were designed to evaluate $PM_{2.5}$ forecast impacts specific to regional meteorological and emission characteristics. The No Wildfire case during July 2014 showed that the Pacific coast regional forecast correlation improved *slightly*, from 0.17 to 0.19 (Fig. 6). The No Dust case for May 2014 showed that Rocky Mountain regional forecasts correlation coefficients improved from 0.12 to 0.27 (Fig. 7). The No J_{NTR}^* 10 case for July showed a negligible impact for $PM_{2.5}$ forecasts and a 3% reduction in O_3 bias in the southeastern United States. The No Snow/Ice run for January

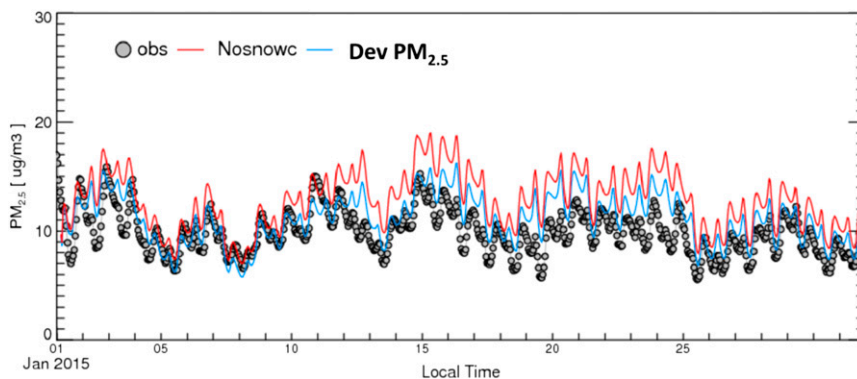


FIG. 8. The $PM_{2.5}$ observed (gray circles) and predicted concentrations ($\mu\text{g m}^{-3}$) for the CONUS averaged over 515 AIRNow stations during January 2015 for the 2015- $PM_{2.5}$ developmental NAQFC $PM_{2.5}$ forecast guidance (blue) and the No Snow/Ice experiment (red).

2015 showed that in the upper Midwest, $PM_{2.5}$ biases were reduced by 52%, from 6.5 to $3.1 \mu\text{g m}^{-3}$ (Fig. 8).

Improvement of $PM_{2.5}$ forecast guidance continues with efforts focusing on the reduction of seasonal (Fig. 4) and diurnal biases (Figs. 5–7) in model predictions. Current efforts by the NAQFC development team seek to improve the physical processes for modeling atmospheric aerosols. Specific current efforts include the incorporation of the latest aerosol sciences from the newest version of CMAQ, incorporation of aerosol plumes that intrude into the CMAQ domain through derivation of the lateral boundary conditions, and application of bias correction techniques based on historical model performance to provide improved forecast guidance for $PM_{2.5}$.

Developmental NAQFC forecast guidance for hourly and 24-h-averaged surface $PM_{2.5}$ concentrations are available online (<http://www.emc.ncep.noaa.gov/mmb/aq/>) and in Gridded Binary (GRIB2) format upon request.

Acknowledgments. This work was partially funded by NOAA's National Air Quality Forecast Capability and the U.S. Weather and Research Program. Throughout this work, the authors appreciate numerous valuable discussions with Drs. Rohit Mathur and Jonathan Pleim of the Atmospheric Modeling and Analysis Division, EPA; Dr. Ariel Stein of NOAA/Air Resources Laboratory; and Drs. Bill Lapenta and Geoff DiMego of the National Centers for Environmental Prediction. We are indebted to the advice of Drs. Mark Q. Liu and Sid Boukabara of the NOAA/National Environmental Satellite, Data, and Information Service. The authors thank the insightful comments from the three anonymous reviewers that added value to this paper. Although this work has been reviewed by NOAA and approved for publication, it does not necessarily reflect NOAA policies or views.

APPENDIX

Equitable Threat Score

Figure A1 shows the annual average ETS for the NAQFC developmental forecast for surface $PM_{2.5}$ averaged over the CONUS with approximately 1000 hourly reporting monitors from the AIRNow surface network between 2010 and 2014. The ETS has been evaluated for the thresholds between 0.5 and $35 \mu\text{g m}^{-3}$. The ETS skill did not improve noticeably over time, especially for the high concentration thresholds.

NAM-Predicted Fields Made Available to CMAQ

Table B1 provides information on the 3D and 2D fields of the output of the NAM output for CMAQ.

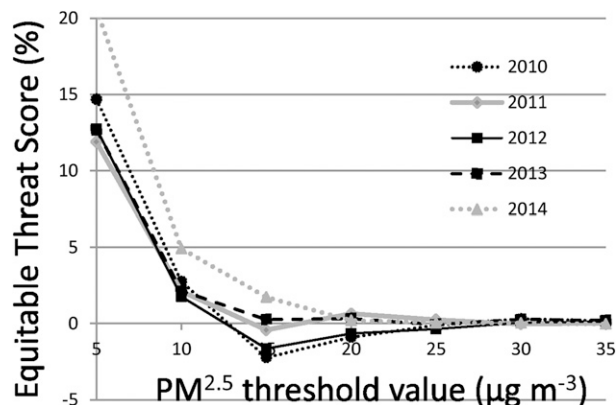


FIG. A1. Annually averaged CONUS-wide ETS at thresholds between 0.5 and $35 \mu\text{g m}^{-3}$ for the NAQFC developmental surface $PM_{2.5}$ forecast verified against approximately 1000 hourly stations from the AIRNow monitoring network between 2010 and 2014.

TABLE B1. NAM-predicted fields made available to CMAQ. Prdgen uses a bilinear interpolation scheme based on the geometrical distance to calculate cross-point values for scalar quantities at midlayers and wind, TKE, and vertical eddy diffusivity values at full layers, except for those variable names labeled with a superscript octothorpe (#), where a nearest-neighbor scheme was used. The variable names that are tagged with a superscript caret (^) are used repeatedly with qualification on vertical levels in accordance with Table 3 (<http://www.nco.ncep.noaa.gov/pmb/docs/on388/table3.html>). Variable definitions are available online (<http://www.nco.ncep.noaa.gov/pmb/docs/on388/table2.html>, <http://www.nco.ncep.noaa.gov/pmb/docs/on388/table129.html>, and <http://www.nco.ncep.noaa.gov/pmb/docs/on388/table130.html>).

	Description (unit)	Variable ID	Table No.
3D variable			
HGT	Geopotential height (m)	7	2
PRES	Pressure (Pa)	1	2
TMP	Temp (K)	11	2
SPFH	Specific humidity (kg kg^{-1})	51	2
UGRD, VGRD	U and V components of wind (m s^{-1})	33, 34	2
VVEL	Vertical velocity (pressure) (Pa s^{-1})	39	2
TCDC	Total cloud cover (%)	71	2
VEDH	Vertical eddy diffusivity heat exchange ($\text{m}^2 \text{s}^{-1}$)	182	129
TKE	Turbulent kinetic energy (J kg^{-1})	158	2
2D variables			
MSLET	Mean sea level pressure (Pa)	130	2
HGT	Terrain height (m)	7	2
TMP [^]	2-m temperature (K)	11	2
SPFH [^]	2-m specific humidity (kg kg^{-1})	51	2
TMP [^]	Skin temp (K)	7	2
UGRD [^] , VGRD [^]	10-m U and V wind components (m s^{-1})	33, 34	2
APCP, NCPCP, ACPCP, WEASD	3-hourly accumulated precipitation: total, large-scale, convective, and water equivalent of snow depth (kg s^{-1})	61, 62, 63, 65	2
TCDC [^]	Total cloud fraction of column (%)	71	2
LHTFL, SHTFL	Instantaneous latent and sensible heat flux (W m^{-2})	121, 122	2
LHTFL [^] , SHTFL [^]	Avg latent and sensible heat fluxes since the last full third hour (W m^{-2})	121, 122	2
TSOIL [^] , SOILM [^]	Soil temp and moisture fraction in the soil layer: 0–10 cm, 10–40 cm, 40 cm–1 m, and 1–2 m (K and kg m^{-2})	85, 86	2
TSOIL [^]	Soil temp at 3 m (K)	85	2
DSWRF, DLWRF, USWRF, ULWRF	Instantaneous downward incoming and upward outgoing short- and longwave radiative fluxes at the surface (W m^{-2})	204, 205, 211, 212	2
DSWRF [^] , DLWRF [^] , USWRF [^] , ULWRF [^]	Avg fluxes as above at the surface since the last full third hour (W m^{-2})	204, 205, 211, 212	2
USWRF [^] , ULWRF [^]	Avg fluxes as above but at the top of the atmosphere (W m^{-2})	211, 212	2
CSDSF	Instantaneous clear-sky downward solar flux (W m^{-2})	161	2
PRES [^] #	Table 3a, level 7; indicates tropopause	1	2
PRES [^]	Table 3a, level 8; indicates model top	1	
PRES [^]	Table 3a, level 110; indicates pressure difference between surface and model top (Pa between NAM's 1st and 60th levels)	1	2
PRES [^]	As above but between beginning of the purely isobaric layer and the model top (Pa)	1	2
FRICV [#]	Friction velocity (m s^{-1})	253	2
CD	Drag coefficient (nondimensional)	252	2
VEG [#]	Vegetative fraction (%)	87	2
ALBDO	Albedo (%)	84	2
WTMP	Water temp (K)	80	2
CNWAT [#]	Plant canopy surface water (kg m^{-2})	223	2
SOTYP	Soil type (Zobler 1999) (0:16)	224	2
VGTYP [#]	Vegetative type (0:18)	225	2
CCOND [#]	Canopy conductance (m s^{-1})	181	130
SFEXC [#]	Exchange coefficient ($\text{kg m}^{-2} \text{s}^{-1}$)	208	130
LAI [#]	Leaf area index (nondimensional)	182	130
HPBL [#]	TKE-based PBL height (m)	221	2
PBLRI [#]	Richardson number–based PBL height (Table 3a, level 220) (m)	7	2
MIXHT [#]	Mixed layer depth (m)	67	2
SNOWC	Snow cover fraction (%)	238	2

REFERENCES

- Aligo, E., B. S. Ferrier, E. Rogers, M. Pyle, S. J. Weiss, and I. L. Jirak, 2014: Modified microphysics for use in high-resolution NAM forecasts. *Proc. 27th Conf. on Severe Local Storms*, Madison, WI, Amer. Meteor. Soc., 16A.1. [Available online at <https://ams.confex.com/ams/27SLS/webprogram/Paper255732.html>.]
- Alpert, J., 2004: Sub-grid scale mountain blocking at NCEP. Preprints, *20th Conf. on Weather Analysis and Forecasting/16th Conf. on Numerical Weather Prediction*, Seattle, WA, Amer. Meteor. Soc., P2.4. [Available online at <https://ams.confex.com/ams/pdfpapers/71011.pdf>.]
- Bey, I., and Coauthors, 2001: Global modeling of tropospheric chemistry with assimilated meteorology: Model description and evaluation. *J. Geophys. Res.*, **106**, 23 073–23 095, doi:10.1029/2001JD000807.
- Bhave, P., G. Sarwar, W. Appel, and R. Dennis, 2006: Revised treatment of N₂O₅ hydrolysis in CMAQ. Preprints, *Fifth Annual CMAS Conf.*, Chapel Hill, NC, Community Modeling and Analysis System. [Available online at <https://www.cmascenter.org/conference/2006/agenda.cfm>.]
- Binkowski, F. S., and U. Shankar, 1995: The regional particulate model 1. Model description and preliminary results. *J. Geophys. Res.*, **100**, 26 191–26 109, doi:10.1029/95JD02093.
- , and S. J. Roselle, 2003: Models-3 Community Multiscale Air Quality (CMAQ) model aerosol component 1. Model description. *J. Geophys. Res.*, **108**, 4183, doi:10.1029/2001JD001409.
- Briggs, G. A., 1972: Chimney plumes in neutral and stable surroundings. *Atmos. Environ.*, **6**, 507–510, doi:10.1016/0004-6981(72)90120-5.
- Brutsaert, W., 1982: *Evaporation into the Atmosphere: Theory, History, and Applications*. D. Reidel, 300 pp.
- Byun, D. W., and R. L. Dennis, 1995: Design artifacts in Eulerian air quality models: Evaluation of the effects of layer thickness and vertical profile correction on surface ozone concentrations. *Atmos. Environ.*, **29**, 105–126, doi:10.1016/1352-2310(94)00225-A.
- , and J. K. S. Ching, Eds., 1999: Science algorithms of the EPA Models-3 Community Multiscale Air Quality (CMAQ) Modeling System. Tech. Rep. EPA-600/R-99/030, Office of Research and Development, U.S. Environmental Protection Agency. [NTIS PB2000-100561.]
- , and K. L. Schere, 2006: Description of the Models-3 Community Multiscale Air Quality (CMAQ) model: System overview, governing equations, and science algorithms. *Appl. Mech. Rev.*, **59**, 51–77, doi:10.1115/1.2128636.
- Canty, T. P., and Coauthors, 2015: Ozone and NO_x chemistry in the eastern US: Evaluation of CMAQ/CB05 with satellite (OMI) data. *Atmos. Chem. Phys.*, **15**, 10 965–10 982, doi:10.5194/acp-15-10965-2015.
- Carlton, A. G., B. J. Turpin, K. E. Altieri, S. P. Seitzinger, R. Mathur, S. J. Roselle, and R. J. Weber, 2008: CMAQ model performance enhanced when in-cloud SOA is included: Comparisons of OC predictions with measurements. *Environ. Sci. Technol.*, **42**, 8798–8802, doi:10.1021/es801192n.
- Chai, T., and Coauthors, 2013: Evaluation of the United States National Air Quality Forecast Capability experimental real-time predictions in 2010 using Air Quality System ozone and NO₂ measurements. *Geosci. Model Dev.*, **6**, 1831–1850, doi:10.5194/gmd-6-1831-2013.
- Chang, J. S., R. A. Brost, I. S. A. Isaksen, S. Madronich, P. Middleton, W. R. Stockwell, and C. J. Walcek, 1987: A three-dimensional Eulerian acid deposition model: Physical concepts and formation. *J. Geophys. Res.*, **92**, 14 681–14 700, doi:10.1029/JD092iD12p14681.
- Colella, P., and P. R. Woodward, 1984: The piecewise parabolic method (PPM) for gas dynamical simulations. *J. Comput. Phys.*, **54**, 174–201, doi:10.1016/0021-9991(84)90143-8.
- Davidson, P., 2009: Research need for air quality forecasting from the NOAA perspective. *First Int. Workshop on Air Quality Forecasting Research*, Boulder CO, NOAA/ESRL. [Available online at http://www.esrl.noaa.gov/csd/events/iwaqfr/presentations/talks/Davidson_Plenary.pdf.]
- Eckermann, S., 2009: Hybrid σ -p coordinate choices for a global model. *Mon. Wea. Rev.*, **137**, 224–245, doi:10.1175/2008MWR2537.1.
- Edney, E. O., T. E. Kleindienst, M. Lewandowski, and J. H. Offenberg, 2007: Updated SOA chemical mechanism for the Community Multi-Scale Air Quality model. Tech. Rep. EPA-600/X-07/025, U.S. EPA, Research Triangle Park, NC, 50 pp.
- Ek, M. B., K. E. Mitchell, Y. Lin, E. Rogers, P. Grunmann, V. Koren, G. Gayno, and J. D. Tarpley, 2003: Implementation of Noah land surface model advances in the National Centers for Environmental Prediction operational mesoscale Eta model. *J. Geophys. Res.*, **108**, 8851, doi:10.1029/2002JD003296.
- EPA, 2005: National air toxics assessment. [Available online at <http://www.epa.gov/ttn/atw/natamain/>.]
- , 2015a: AIRNow—Air quality monitor maps. [Available online at <http://www.airnow.gov/index.cfm?action=airnow.pointmaps>.]
- , 2015b: National Ambient Air Quality Standards for Ozone—Proposed rule. *Fed. Regist.*, **79**, 75 234–75 411. [Available online at <http://www.gpo.gov/fdsys/pkg/FR-2014-12017/pdf/2014-28674.pdf>.]
- Fann, N., A. D. Lamson, S. Anenberg, K. Wesson, D. Risley, and B. J. Hubbell, 2012: Estimating the national public health burden associated with exposure to ambient PM_{2.5} and ozone. *Risk Anal.*, **32**, 81–95, doi:10.1111/j.1539-6924.2011.01630.x.
- Gandin, L. S., and A. H. Murphy, 1992: Equitable skill scores for categorical forecasts. *Mon. Wea. Rev.*, **120**, 361–370, doi:10.1175/1520-0493(1992)120<0361:ESSFCF>2.0.CO;2.
- Hsu, Y., and F. Divita Jr., 2011: SPECIATE 4.3: Addendum to SPECIATE4.2: Speciation data base development documentation. EPA Tech. Rep. EPA/600/R-11/121, 27 pp. [Available online at <https://www3.epa.gov/ttn/chief/software/speciate/speciate4/addendum4.2.pdf>.]
- Janjić, Z. I., 1990: The step-mountain coordinates: Physical package. *Mon. Wea. Rev.*, **118**, 1429–1443, doi:10.1175/1520-0493(1990)118<1429:TSMCPP>2.0.CO;2.
- , 1994: The step-mountain eta coordinate model: Further developments of the convection, viscous sublayer, and turbulence closure schemes. *Mon. Wea. Rev.*, **122**, 927–945, doi:10.1175/1520-0493(1994)122<0927:TSMCEM>2.0.CO;2.
- , 2000: Comments on “Development and evaluation of a convection scheme for use in climate models.” *J. Atmos. Sci.*, **57**, 3686, doi:10.1175/1520-0469(2000)057<3686:CODAEO>2.0.CO;2.
- , and R. Gall, 2012: Scientific documentation of the NCEP Nonhydrostatic Multiscale Model on the B grid (NMMB). Part 1 Dynamics. NCAR Tech. Note NCAR/TN-489+STR, 75 pp. [Available online at <https://opensky.ucar.edu/islandora/object/technotes%3A502/datastream/PDF/view>.]
- , J. P. Gerrity Jr., and S. Nickovic, 2001: An alternative approach to nonhydrostatic modeling. *Mon. Wea. Rev.*, **129**, 1164–1178, doi:10.1175/1520-0493(2001)129<1164:AAATNM>2.0.CO;2.
- Kelly, J. T., P. V. Bhave, C. G. Nolte, U. Shankar, and K. M. Foley, 2009: Simulating emission and chemical evolution of coarse sea-salt particles in the Community Multiscale Air Quality

- (CMAQ) model. *Geosci. Model Dev.*, **2**, 1335–1374, doi:[10.5194/gmdd-2-1335-2009](https://doi.org/10.5194/gmdd-2-1335-2009).
- Larkin, N. K., and Coauthors, 2009: The BlueSky smoke modeling framework. *Int. J. Wildland Fire*, **18**, 906–920, doi:[10.1071/WF07086](https://doi.org/10.1071/WF07086).
- Lee, P., and F. Ngan, 2011: Coupling of important physical processes in the planetary boundary layer between meteorological and chemistry models for regional to continental scale air quality forecasting: An overview. *Atmosphere*, **2**, 464–483, doi:[10.3390/atmos2030464](https://doi.org/10.3390/atmos2030464).
- , and Coauthors, 2009: Impact of consistent boundary layer mixing approaches between NAM and CMAQ. *Environ. Fluid Mech.*, **9**, 23–42, doi:[10.1007/s10652-008-9089-0](https://doi.org/10.1007/s10652-008-9089-0).
- Lefsky, M. A., 2010: A global forest canopy height map from the Moderate Resolution Imaging Spectroradiometer and the Geoscience Laser Altimeter System. *Geophys. Res. Lett.*, **37**, L15401, doi:[10.1029/2010GL043622](https://doi.org/10.1029/2010GL043622).
- Mathur, R., S. Yu, D. Kang, and K. L. Schere, 2008: Assessment of the wintertime performance of developmental particulate matter forecasts with the Eta-Community Multiscale Air Quality modeling system. *J. Geophys. Res.*, **113**, D02303, doi:[10.1029/2007JD008580](https://doi.org/10.1029/2007JD008580).
- Mitchell, K. E., and Coauthors, 2004: The multi-institution North American Land Data Assimilation System (NLDAS): Utilizing multiple GCIIP products and partners on a continental distributed hydrological modeling system. *J. Geophys. Res.*, **109**, D07S90, doi:[10.1029/2003JD003823](https://doi.org/10.1029/2003JD003823).
- Mlawer, E. J., S. J. Taubman, P. D. Brown, M. J. Iacono, and S. A. Clough, 1997: Radiative transfer for inhomogeneous atmosphere: RTTM, a validated correlated-k model for the longwave. *J. Geophys. Res.*, **102**, 16 663–16 682, doi:[10.1029/97JD00237](https://doi.org/10.1029/97JD00237).
- Nenes, A., S. N. Pandis, and C. Pilinis, 1998: ISORROPIA: A new thermodynamic equilibrium model for multiphase multicomponent inorganic aerosols. *Aquat. Geochem.*, **4**, 123–152, doi:[10.1023/A:1009604003981](https://doi.org/10.1023/A:1009604003981).
- O'Neill, S. M., and Coauthors, 2009: Regional real-time smoke prediction systems. *Wildland Fires and Air Pollution*, A. Bytnerowicz et al., Eds., Developments in Environmental Science, Vol. 8, Elsevier, 499–534.
- Otte, T. L., and J. E. Pleim, 2010: The Meteorology-Chemistry Interface Processor (MCIP) for the CMAQ modeling system: Updates through MCIPv3.4.1. *Geosci. Model Dev.*, **3**, 243–256, doi:[10.5194/gmd-3-243-2010](https://doi.org/10.5194/gmd-3-243-2010).
- , and Coauthors, 2005: Linking the Eta Model with the Community Multiscale Air Quality (CMAQ) modeling system to build a National Air Quality Forecasting System. *Wea. Forecasting*, **20**, 367–384, doi:[10.1175/WAF855.1](https://doi.org/10.1175/WAF855.1).
- Owen, P. R., 1964: Saltation of uniform grains in air. *J. Fluid Mech.*, **20**, 225–242, doi:[10.1017/S0022112064001173](https://doi.org/10.1017/S0022112064001173).
- Pan, L., D. Q. Tong, P. Lee, H. Kim, and T. Chai, 2014: Assessment of NO_x and O₃ forecasting performances in the U.S. National Air Quality Forecasting Capability before and after the 2012 major emissions updates. *Atmos. Environ.*, **95**, 610–619, doi:[10.1016/j.atmosenv.2014.06.020](https://doi.org/10.1016/j.atmosenv.2014.06.020).
- Pasquill, F., and F. B. Smith, 1983: *Atmospheric Diffusion*. 3rd ed. E. Horwood, 437 pp.
- Pleim, J. E., 2007a: A combined local and nonlocal closure model for the atmospheric boundary layer. Part I: Model description and testing. *J. Appl. Meteor. Climatol.*, **46**, 1383–1395, doi:[10.1175/JAM2539.1](https://doi.org/10.1175/JAM2539.1).
- , 2007b: A combined local and nonlocal closure model for the atmospheric boundary layer. Part II: Application and evaluation in a mesoscale meteorological model. *J. Appl. Meteor. Climatol.*, **46**, 1396–1409, doi:[10.1175/JAM2534.1](https://doi.org/10.1175/JAM2534.1).
- , A. Xiu, P. L. Finkelstein, and J. F. Clarke, 1997: Evaluation of a coupled land-surface and dry deposition model through comparison to field measurements of surface heat, moisture, and ozone fluxes. Preprints, *12th Symp. on Boundary Layer and Turbulence*, Vancouver, BC, Canada, Amer. Meteor. Soc., 478–479.
- Ruminski, M., S. Kondragunta, R. Draxler, and J. Zeng, 2006: Recent change to the Hazard Mapping System. Preprints, *15th Int. Emission Inventory Conf.: Reinventing Inventories—New Ideas in New Orleans*, New Orleans, LA, NOAA/Office of Air Quality Planning and Standards. [Available online at <https://www3.epa.gov/ttn/chieff/conference/ei15/finalprogram.pdf>.]
- Saylor, R. D., and A. F. Stein, 2012: Identifying the causes of differences in ozone production from the CB05 and CBMIV chemical mechanisms. *Geosci. Model Dev.*, **5**, 257–268, doi:[10.5194/gmd-5-257-2012](https://doi.org/10.5194/gmd-5-257-2012).
- Schwede, D., G. Pouliot, and T. Pierce, 2005: Changes to the Biogenic Emissions Inventory System Version 3 (BEIS3). Preprints, *Fourth CMAS Models-3 Users' Conf.*, Chapel Hill, NC, Community Modeling and Analysis System. [Available online at https://www.cmascenter.org/conference/2005/abstracts/2_7.pdf.]
- Stajner, I., P. Davidson, D. Byun, J. McQueen, R. Draxler, P. Dickerson, and J. Meagher, 2012a: US National Air Quality Forecast Capability: Expanding coverage to include particulate matter. *Air Pollution Modeling and Its Application XXI*, D. G. Steyn and S. T. Castelli, Eds., Springer, 379–384, doi:[10.1007/978-94-007-1359-8_64](https://doi.org/10.1007/978-94-007-1359-8_64).
- , J. McQueen, P. Lee, R. Draxler, P. Dickerson, and K. Wedmark, 2012b: Recent performance of the National Air Quality Forecast Capability. Preprints, *11th Annual CMAS Conf.*, Chapel Hill, NC, Community Modeling and Analysis System, 379–384.
- , and Coauthors, 2014: National Air Quality Forecast Capability: Recent progress and plans. Preprints, *13th Annual CMAS Conf.*, Chapel Hill, NC, Community Modeling and Analysis System. [Available online at <https://www.cmascenter.org/conference/2014/agenda.cfm>.]
- Tager, I. B., J. Balmes, F. Lurmann, L. Ngo, S. Alcorn, and N. Künzli, 2005: Chronic exposure to ambient ozone and lung function in young adults. *Epidemiology*, **16**, 751–759, doi:[10.1097/01.ede.0000183166.68809.b0](https://doi.org/10.1097/01.ede.0000183166.68809.b0).
- Tang, Y., and Coauthors, 2009: The impact of lateral boundary conditions on CMAQ predictions over the continental United States. *Environ. Fluid Mech.*, **9**, 43–58, doi:[10.1007/s10652-008-9092-5](https://doi.org/10.1007/s10652-008-9092-5).
- Tong, D. Q., G. E. Bowker, S. He, R. Mathur, and D. A. Gillette, 2015a: Development of a windblown dust module within the Community Multiscale Air Quality (CMAQ) model: Description and preliminary applications in the continental United States. *Atmos. Environ.*, **107**, 70–84, doi:[10.1016/j.atmosenv.2015.01.035](https://doi.org/10.1016/j.atmosenv.2015.01.035).
- , and Coauthors, 2015b: Long-term NO_x trends over large cities in the United States during the 2008 recession: Intercomparison of satellite retrievals, ground observations, and emission inventories. *Atmos. Environ.*, **107**, 70–84, doi:[10.1016/j.atmosenv.2015.01.035](https://doi.org/10.1016/j.atmosenv.2015.01.035).
- Wu, W.-S., R. J. Purser, and D. F. Parrish, 2002: Three-dimensional variational analysis with spatially inhomogeneous covariances. *Mon. Wea. Rev.*, **130**, 2905–2916, doi:[10.1175/1520-0493\(2002\)130<2905:TDVAWS>2.0.CO;2](https://doi.org/10.1175/1520-0493(2002)130<2905:TDVAWS>2.0.CO;2).
- Yarwood, G., S. Rao, M. Yocke, and G. Whitten, 2005: Updates to the carbon bond chemical mechanism: CB05. Final Rep. to the US EPA, RT-0400675. [Available online at http://www.camx.com/publ/pdfs/cb05_final_report_120805.pdf.]
- Zobler, L., 1999: Global soil types, 1-degree grid (Zobler). Oak Ridge National Laboratory Distributed Active Archive Center, Oak Ridge, TN, doi:[10.3334/ORNLDAAAC/418](https://doi.org/10.3334/ORNLDAAAC/418).